HHS Public Access

Author manuscript

Biochemistry. Author manuscript; available in PMC 2016 March 30.

Published in final edited form as:

Biochemistry. 2015 October 20; 54(41): 6402–6412. doi:10.1021/acs.biochem.5b00505.

Probing Structural Dynamics and Topology of the KCNE1 Membrane Protein in Lipid Bilayers via Site-Directed Spin Labeling and Electron Paramagnetic Resonance Spectroscopy

Indra D. Sahu[†], **Andrew F. Craig**[†], **Megan M. Dunagan**[†], **Kaylee R. Troxel**[†], **Rongfu Zhang**[†], **Andrew G. Meiberg**[†], **Corrinne N. Harmon**[†], **Robert M. McCarrick**[†], **Brett M. Kroncke**[‡], **Charles R. Sanders**[‡], and **Gary A. Lorigan**[*,†]

[†]Department of Chemistry and Biochemistry, Miami University, Oxford, Ohio 45056, United States

[‡]Department of Biochemistry and Center for Structural Biology, Vanderbilt University, Nashville, Tennessee 37232, United States

Abstract

KCNE1 is a single transmembrane protein that modulates the function of voltage-gated potassium channels, including KCNQ1. Hereditary mutations in the genes encoding either protein can result in diseases such as congenital deafness, long QT syndrome, ventricular tachyarrhythmia, syncope, and sudden cardiac death. Despite the biological significance of KCNE1, the structure and dynamic properties of its physiologically relevant native membrane-bound state are not fully understood. In this study, the structural dynamics and topology of KCNE1 in bilayered lipid vesicles was investigated using site-directed spin labeling (SDSL) and electron paramagnetic resonance (EPR) spectroscopy. A 53-residue nitroxide EPR scan of the KCNE1 protein sequence including all 27 residues of the transmembrane domain (45–71) and 26 residues of the N- and C-termini of KCNE1 in lipid bilayered vesicles was analyzed in terms of nitroxide side-chain motion. Continuous wave-EPR spectral line shape analysis indicated the nitroxide spin label side-chains located in the KCNE1 TMD are less mobile when compared to the extracellular region of KCNE1. The EPR data also revealed that the C-terminus of KCNE1 is more mobile when compared to the N-terminus. EPR power saturation experiments were performed on 41 sites including 18 residues previously proposed to reside in the transmembrane domain (TMD) and 23 residues of the N- and C-termini to determine the topology of KCNE1 with respect to the 1-palmitoyl-2-oleoyl-*sn*-glycero-3-phosphocholine (POPC)/1-palmitoyl-2-oleoyl-*sn*-glycero-3-phospho-(1′-*rac*-glycerol) (POPG) lipid bilayers. The results indicated that the transmembrane domain is indeed buried within the membrane, spanning the width of the lipid bilayer. Power saturation data also revealed that the extracellular region of KCNE1 is solvent-exposed with some

[*]**Corresponding Author:**gary.lorigan@miamioh.edu. Phone: (513) 529-3338.

Supporting Information

The Supporting Information is available free of charge on the ACS Publications website at DOI: 10.1021/acs.biochem.5b00505. CW-EPR spectral simulation of KCNE1 mutants (Figure S1), CW-EPR spectra on KCNE1 mutants in micelles and liposomes (Figure S2), and rotational correlation times and relative population of two spectral components of EPR spectra (Table S1) (PDF)

Notes

The authors declare no competing financial interest.

of the portions partially or weakly interacting with the membrane surface. These results are consistent with the previously published solution NMR structure of KCNE1 in micelles.

Graphical abstract

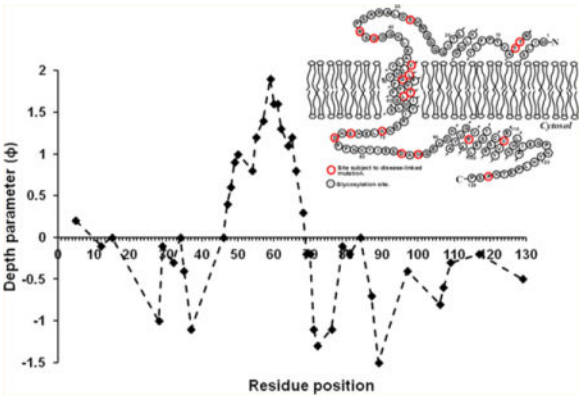

Voltage-gated ion channels are essential for the electrical excitability of neurons, muscles, and other excitable cells.[1] KCNE1 is a transmembrane protein consisting of 129 amino acids that modulates the function of a voltage-gated potassium ion channel (K_v).[2] Voltage-gated K^+ channels are critical for the function of cardiac, nervous, and auditory systems and are promising targets for various therapeutic agents.[3–5] In the human heart, KCNQ1 associates with KCNE1 to generate the slow delayed rectifier current (I_{Ks}), characterized by its slow activation and deactivation kinetics,[6] which is essential for the repolarization phase of the cardiac action potential. Mutations in these genes cause changes in the function of the KCNE1/KCNQ1 complex resulting in increased susceptibility to diseases such as congenital deafness, congenital long QT syndrome (LQTS), ventricular tachyarrhythmia, syncope, and sudden cardiac death.[7–9] The structure and dynamics of the I_{Ks}-producing complex in the physiologically relevant native membrane-bound state are not fully understood. However, the structure of KCNE1 was recently determined in 1-myristoyl-2-hydroxy-*sn*-glycero-3-phospho-(1′-*rac*-glycerol) (LMPG) detergent micelles, where its transmembrane domain was observed to have a curved α-helix, with both N- and C-termini consisting of flexibly linked α-helices, some of which have an affinity for the micellar surface.[2]

Detergent micelles are often used as membrane-mimetics for membrane proteins due to their small size, facilitating high-resolution structure analysis by solution NMR spectroscopy. However, it is often difficult to test whether the structure of proteins in a micelle environment is the same as the membrane-bound form. Detergent micelles have recently come under considerable criticism as model membranes on the basis that they sometimes distort membrane protein structures from their true native like forms.[10,11] Circular dichroism (CD) spectroscopic data indicated that the percentage of α-helical content for KCNE1 is higher in reconstituted 1-palmitoyl-2-oleoyl-*sn*-glycero-3-phosphocholine (POPC)/1-palmitoyl-2-oleoyl-*sn*-glycero-3-phospho-(1′-*rac*-glycerol) (POPG) lipid vesicles than in LMPG micelles indicating that KCNE1 has increased regular secondary structure in the more native-like environment of lipid bilayers.[12] On the other hand, recent EPR double electron-electron resonance (DEER) data demonstrated that the KCNE1 transmembrane

domain (TMD) adopts an α-helical structure with slight curvature in lipid vesicles, consistent with the NMR structure in micelles, with the curvature appearing to be critical for the KCNE1 function.[2,7,13,14] It is clearly important to study the details of the structural and dynamic properties of KCNE1 in a physiologically relevant, more native, membrane-bound environment to elucidate which features of the NMR structure reflect native properties and which features reflect micellar distortions.

In this study, continuous wave electron paramagnetic resonance (CW-EPR) spectroscopy was used to investigate the dynamics and structural topology of the full-length KCNE1 protein in POPC/POPG phospholipid vesicles. CW-EPR spectra obtained from a series of 53 single sites of KCNE1 covering the TMD (45–71), and several sites on the C-and N-termini in POPC/POPG proteoliposomes were qualitatively and quantitatively analyzed to determine the nitroxide side-chain mobility and nitroxide side-chain dynamics. Moreover, EPR power saturation data were obtained on a series of 41 single mutants including 18 mutations on the TMD and 23 outside mutants including both the N-and C-termini of KCNE1. The dynamic properties and location of these spin-labeled KCNE1 mutants with respect to the membrane were studied.

MATERIALS AND METHODS

Site-Directed Mutagenesis

The His_6-tag expression vectors (pET-16b) containing the cDNA for wild type KCNE1 and a cysteine-less mutant form were transformed into XL1-Blue *Escherichia coli* cells (Stratagene). Plasmid extracts from these cells were obtained using the QIAprep Spin Miniprep kit (Qiagen). Site-directed cysteine mutants were introduced into the cysteine-less KCNE1 gene using the QuickChange Lightning Site-Directed Mutagenesis kit (Stratagene). The KCNE1 mutations were confirmed by DNA sequencing from XL10-Gold *E. coli* (Stratagene) transformants using the T7 primer (Integrated DNA Technologies). Successfully mutated vectors were transformed into BL21-(DE3) CodonPlus-RP *E. coli* cells (Stratagene) for protein overexpression. A series of 53 single substitution mutants were prepared that correspond to residues 45–71 of the transmembrane domain, residues 3, 5, 9, 12, 15, 21, 28, 29, 32, 33, 34, 35, and 37 of the N-terminus, and residues 72, 76, 79, 87, 89, 95, 102, 104, 106, 107, 109, 117, and 129 of the C-terminal of the KCNE1 sequence. These mutants were selected to represent all domains of KCNE1.

Overexpression and Purification

Overexpression of wild type and mutant forms of KCNE1 in *E. coli* BL21 cells was carried out using a previously described protocol.[7,12] Purification of KCNE1 from inclusion bodies isolated from these cells was carried out according to a previously described method[7,12] with final purification into 0.05% LMPG detergent solutions. Protein concentration was determined from the OD_{280} using an extinction coefficient of 1.2 mg/mL protein per OD_{280} on a NanoDrop 200c (Thermo Scientific). The purity of protein was confirmed by sodium dodecyl sulfate polyacrylamide gel electrophoresis (SDS-PAGE).

Spin Labeling and Reconstitution into Proteoliposomes

Spin labeling and reconstitution into proteoliposomes were carried out following a previously described protocol.[15] After purification, each cysteine mutant was concentrated to 0.5 mM, and the pH was lowered to 6.5. Samples were then reduced with 2.5 mM DTT, with gentle agitation at room temperature for 24 h to ensure complete conversion to Cys-SH. MTSL spin label was added to 10 mM from a 250 mM stock solution in methanol into 0.5 mM KCNE1 solution, which was then gently agitated at room temperature for 30 min, followed by incubation at 37 °C for 3 h and then overnight at room temperature. Samples were next buffer-exchanged into a 50 mM phosphate, 0.05% LMPG, pH 7.8. Following buffer exchange, samples were bound to Ni(II) resin in a column, which was then washed with 200 mL of 50 mM phosphate, 0.05% LMPG, pH 7.8 to remove excess MTSL. The spin-labeled KCNE1 was re-eluted using elution buffer (250 mM IMD, 100 NaCl, 20 mM Tris, pH 7.8) with 0.5% SDS detergent. The spin labeling efficiency was determined by comparing the nanodrop UV A_{280} protein concentration with the spin concentration obtained from CW-EPR spectroscopy. The spin labeling efficiency for all samples was ~75–80%.

The reconstitution of spin labeled protein into POPC/POPG (3:1) vesicles was carried out via dialysis-based methods following a similar protocol in the literature.15,16 The concentrated spin labeled KCNE1 protein was mixed with a stock lipid mixture (400 mM SDS, 75 mM POPC and 25 mM POPG, 0.1 mM EDTA, 100 mM IMD, pH 6.5). The lipid mixture was pre-equilibrated to form clear mixed micelles via extensive freeze/thaw cycles. The final protein/lipid molar ratio was set to 1:400. The KCNE1-lipid mixture was then subjected to extensive dialysis to remove all SDS, during which process KCNE1/POPC/POPG vesicles spontaneously formed. The 4 L of dialysis buffer (10 mM IMD and 0.1 mM EDTA at pH 6.5) was changed two times daily. The completion of SDS removal was determined when the KCNE1-lipid solution became cloudy and the surface tension of the dialysate indicated complete removal of detergent.

EPR Spectroscopic Measurements

EPR experiments were conducted at the Ohio Advanced EPR Laboratory at Miami University. CW-EPR spectra were collected at X-band on a Bruker EMX CW-EPR spectrometer using an ER041xG microwave bridge and ER4119-HS cavity coupled with a BVT 3000 nitrogen gas temperature controller. The spin concentration for KCNE1 samples was ~80–100 μM. Each spin-labeled CW-EPR spectrum was acquired by signal averaging 10 42-s field scans with a central field of 3315 G and sweep width of 100 G, modulation frequency of 100 kHz, modulation amplitude of 1 G, and microwave power of 10 mW at 295 K. The side-chain mobility was determined by calculating the inverse central line width from each CW-EPR spectrum.

An empirical motional parameter (τ_0) was determined from the CW-EPR spectra using eq 1.[17–20]

$$\tau_0 = K \times \Delta H \left[\left(\frac{h_0}{h_{(-1)}} \right)^{1/2} - 1 \right] \quad (1)$$

where $K = 6.5 \times 10^{-10}$ s, ΔH is the width of the center-line, and h_0 and h_{-1} are the heights of the center and high field lines, respectively.

EPR Spectral Simulations

EPR spectra were simulated using the Multicomponent LabVIEW program written by Dr. Christian Altenbach[21] including the macroscopic order, microscopic disorder (MOMD) model developed by Freed group.[22,23] The principal components of the hyperfine interaction tensor A = [5.5 G, 5.5 G, 34.8 G] and g-tensors g = [2.0088, 2.0063, 2.0023] were obtained from a least-square fit to the spectrum of V50C KCNE1 in a frozen state at 150 K. During the simulation process, the A and g tensors were held constant, and the rotational diffusion tensors were varied. A two-site fit was used to account for both the rigid/slower and higher/faster motional components of the EPR spectrum. The best fit rotational correlation times and relative population of both components were determined using a Brownian diffusion model.

CW-EPR Power Saturation Measurements

Power saturation experiments were performed on a Bruker EMX X-band CW-EPR spectrometer consisting of an ER 041XG microwave bridge coupled with an ER 4123D CW-Resonator (Bruker BioSpin) following a previously described procedure.[12] Samples were loaded into gas permeable TPX capillary tubes with a total volume of 3–4 μL at a concentration of 40–60 μM. EPR data collection was carried out using a modulation amplitude of 1 G and a varying microwave power of 0.4–100 mW. The scan range of all spectra was 100 G, and the final spectra were obtained by signal averaging 10 scans.

CW-EPR power saturation curves were obtained for 18 mutants of the supposed transmembrane domain (probe inside model membrane) and 23 mutants of the extracellular region (probe outside) on KCNE1 under three conditions: (1) equilibrated with nitrogen as a control; (2) equilibrated with a lipid-soluble paramagnetic reagent: air (20% oxygen); and (3) equilibrated with nitrogen in the presence of a water-soluble paramagnetic reagent nickel(II) ethylenediaminediacetate (NiEDDA chelate (1 mM), as previously synthesized.[24] The samples were purged with gas for at least 60 min at a rate of 10 mL/min before performing each EPR measurement. High purity nitrogen and house supply compressed air lines were used. The resonator remained connected to the gas line during all measurements, and the sample temperature was held at 295 K. The peak-to-peak amplitude of the first derivative $m_I = 0$ resonance line (A) was measured and plotted against the square root of the incident microwave power. The data points were then fit using a Matlab software script using eq 2:

$$A = I\sqrt{P}\left[1 + (2^{1/\varepsilon} - 1)P/P_{1/2}\right]^{-\varepsilon} \quad (2)$$

where I is a scaling factor, $P_{1/2}$ is the power where the first derivative amplitude is reduced to half of its unsaturated value, and ε is a measure of the homogeneity of saturation of the resonance line. In eq 2, I, ε, and $P_{1/2}$ are adjustable parameters and yield a characteristic $P_{1/2}$ value. The corresponding Φ depth parameters were calculated using eq 3.[25–28]

$$\Phi = ln\left(\frac{\Delta P_{1/2}(O_2)}{\Delta P_{1/2}(\mathrm{NiEDDA})}\right) \quad (3)$$

where $\Delta P_{1/2}(O_2)$ is the difference in the $P_{1/2}$ values for air- and nitrogen-exposed samples, and $\Delta P_{1/2}$(NiEDDA) is the difference in the $P_{1/2}$ values for NiEDDA and nitrogen-exposed samples.

The location of residues of the transmembrane domain of KCNE1 inside the membrane (membrane depth (Å)) was calculated using the bilayer depth calibration equation: (depth (Å) = 5.6 φ + 2.3) previously determined in our lab.[12]

RESULTS

The structural dynamics and topology of KCNE1 in POPC/POPG lipid bilayers were investigated using SDSL coupled with EPR spectroscopy. Both CW-EPR line shape analysis and CW-EPR power saturation methods were used to probe KCNE1. For these studies a POPC/POPG (3:1) lipid bilayer was used to mimic phospholipids typically found in mammalian membranes.[12,15,16,29] Functional studies of KCNE1 with KCNQ1 in POPC/POPG lipid bilayers under similar sample conditions have shown K^+ channel activity.[12] Figure 1 displays the schematic representation of the MTSL spin-label (Figure 1A), the proposed topology of the KCNE1 sequence in lipid bilayers (Figure 1B), and the KCNE1 amino acid sequence with the location of spin-labeling sites (Figure 1C) used in this study.

Structural Dynamics of KCNE1 using CW-EPR Line-shape Analysis

Nitroxide based site-directed spin labeling (SDSL) coupled with EPR is a very powerful tool to study the structure and conformational dynamics of membrane proteins in a lipid bilayer environment.[16,20,30,31] Analysis of CW-EPR data for a series of spin-labeled protein sequences allows modeling of the protein structure with a spatial resolution at the residue-specific level.[32–35] The dynamics of KCNE1 were investigated by analyzing the line shape of CW-EPR spectra obtained for 53 spin labeled derivatives of KCNE1 mutants in multilamellar vesicles (MLVs). These sites were chosen to cover the full span of the transmembrane domain (45–71 based on previous work), the N-terminal domain (3, 5, 9, 12, 15, 21, 28, 29, 32, 33, 34, 35, and 37) and the C-terminal domain (72, 76, 79, 87, 89, 95, 102, 104, 106, 107, 109, 117, and 129) of KCNE1.[2] Figure 2 shows CW-EPR spectra for each KCNE1 mutant in POPC/POPG proteoliposomes at 295 K. Two different spectral components were observed in a majority of the EPR data, as indicated by two vertical arrows. The left arrows reflect rigid/slower components, while the right arrows shows higher/faster motional components. These motional components may arise due to the contribution of multiple conformations of the spin-label rotamers, backbone fluctuation of KCNE1, and multiple conformational states of KCNE1 interacting with the lipid bilayer.[36] The KCNE1 CW-EPR spectra are consistent with previously published CW-EPR data for a

variety of different membrane proteins in proteoliposomes.[37–41] Inspection of the EPR spectral line-shapes indicates that different segments of KCNE1 interact differently with the lipid bilayers as observed by the variation in line broadenings for different spin-labeling positions. The two motional components are easily discerned in the EPR spectra for sites located in the extracellular (N-terminal) region of the KCNE1 sequence (Figure 2A). EPR spectra of spin-labeled sites located in the C-terminus also exhibit two spectral components (Figure 2C), which are even more prominent than spectra from sites located at the N-terminus. The EPR line widths are broader for the TMD spin-labeled mutants of KCNE1, when compared to that in the N- and C-termini.

In order to quantify the side-chain mobility of the spin-labeling sites, the inverse of the central line width was calculated from each spectrum and plotted as a function of the residue number (see Figure 3). The inverse central line width of the TMD of KCNE1 varies between 0.24 G^{-1} to 0.38 G^{-1}, while the extracellular region varies between 0.30 G^{-1} to 0.66 G^{-1}. Interestingly, the inverse central line width for the C-terminus of KCNE1 was higher than that of the N-terminus of KCNE1. The sharpest line shape was observed for residue 129 with an inverse line width of 0.66 G^{-1} suggesting that this position is very mobile. Figure 3 clearly indicates that the TMD of KCNE1 (45–71) has the smaller inverse central line width or broadest line width periodicity pattern profile when compared to the N-and C-termini while the C-terminus has the overall largest inverse central line width profile compared to N-terminus. This suggests that the KCNE1 TMD is buried within the lipid bilayers and interacts strongly with the lipid hydrophobic acyl chain while the N-terminus and C-terminus are solvent exposed and partially or weekly interacting with the lipid bilayer surface. The lower mobility profile of the N-terminus when compared to the C-terminus indicates that the N-terminus may be interacting more closely with the lipid bilayer surface when compared to the C-terminus region. This is consistent with the NMR relaxation measurements reported for the protein in micelles.[7] The inverse central line width profile of KCNE1 is consistent with previously published mobility profiles for integral membrane proteins.[42]

In order to further explore the side-chain dynamics of spin-labeled KCNE1, an empirical motional parameter (τ_0), was measured for each residue according to eq 1. The data are plotted in Figure 4. The motional parameter of the TMD of KCNE1 varies from 2.6 to 6.3 ns, while the extracellular region varies between 0.5 to 4.5 ns. Figure 4 clearly indicates that τ_0 for TMD of KCNE1 is higher than that of extracellular region. The motional parameter pattern for the C-terminus region is lower when compared to the N-terminus. The τ_0 parameter pattern suggests that the spin-labeled KCNE1 TMD side-chains are tumbling slowly when compared to the extracellular termini, with the C-terminus side-chains tumbling faster than the N-terminal sites. This motional parameter pattern is consistent with the spin-label side-chain mobility of the corresponding mutants from Figure 3.

In order to determine the nature of the two major components observed in the EPR spectra of KCNE1, the effect of osmolyte perturbation was investigated at different sites. 30% sucrose was used as the osmolyte as previously described in the literature.[43] For solvent exposed spin-labeled sites with two major components, protein conformational states have different solvent accessible surface areas and the interaction of osmolytes shift the

equilibrium among the substates, resulting in significant changes in the complex EPR spectra of the MTSL spin-labeled side-chain. However, if the two major components EPR spectra arise from a series of different spin-label rotamers in equilibria, they are insensitive to the osmolytes due to the small difference in solvent exposed area of the protein for different spin-label rotamers.[43] In this case, no changes are observed in the EPR spectra upon addition of an osmolyte. Figure 5 shows CW-EPR spectra of R33C, E89C, and V109C KCNE1 with and without 30% sucrose. These residues are solvent exposed and will interact with the sucrose. The EPR spectra clearly show significant spectral line shape changes upon addition of 30% sucrose. The addition of 30% sucrose caused an increase shift in population of the more rigid spectral component for all three solvent exposed sites. The spectral changes observed are comparable to other solvent exposed sites in the literature.[43] The results indicate that the two major components observed in the EPR spectra are likely due to conformational exchange between different substates, and not from different spin-label rotamers.

In order to further quantify the spin-label side-chain motion of KCNE1, NLSL MOMD EPR spectral simulations were carried out on representative EPR spectra of sites V50C and I66C from the transmembrane domain, F12C from the N-terminus, and site D76C from the C-terminus to determine the correlation times and relative population of the different components. The multicomponent LabVIEW program developed by Christian Altenbach (http://www.biochemistry.ucla.edu/biochem/Faculty/Hubbell/) was used for the study.[21–23] The Zeeman interaction tensors (g_{xx}, g_{yy}, g_{zz}) and hyperfine interaction tensors (A_{xx}, A_{yy}, A_{zz}) were held constant during the fitting process and the correlation times and relative population of the two components were determined from the best fit EPR spectra (see Figure S1 and Table S1). The simulation results indicated that the mobile and rigid components for the transmembrane mutants (V50C and I66C) are slower with longer correlation times 1.2 ns and a relative population of 74% (motional component) and 13.7 ns of 26% (rigid component) for site V50C, and 1.1 ns with relative population of 76% (motional component) and 16.1 ns of 24% (rigid component) for site I66C. The outside solvent exposed mutants (F12C, D76C) have correlation times of 0.8 ns with a relative population of 55% (motional component) and 8.2 ns with a relative population of 45% (rigid component).

CW-EPR data were also collected on 12 representative sites covering different sections of KCNE1 including the N-terminus (L3C, R33C, S37C), transmembrane domain (V50C, F53C, F56C, I66C), and the C-terminus (D76C, E89C, K104C, V109C, P129C) in 7.5% LMPG micelles for comparison with liposomes (Figure S2). The CW-EPR line shape of KCNE1 in LMPG micelles are generally not as broad as the liposome data shown in Figure 2 and mostly consisted of a single component. The KCNE1 EPR spectra are consistent with previously published EPR data of integrin β_{1a} incorporated into both liposomes and micelle complexes.[41] The CW-EPR data also revealed that P129C has a very mobile spectral line shape similar to that of the same sample in liposomes (see Figure 2) indicating that the spin-label motion of P129C is similarly faster in both micelles and lipid bilayers, when compared to the other sites. These results also support our osmolyte perturbation result that the two major components observed in the EPR spectra of KCNE1 in lipid bilayers are most likely

due to protein conformational exchange upon interaction of different segments of the protein with the membrane.

Topology of KCNE1 with Respect to the Membrane

CW-EPR power saturation experiments were performed on spin-labeled KCNE1 samples to examine the locations and insertion depth of various residues and segments with respect to the membrane. CW-EPR power saturation experiments can monitor the relaxation rate of spin-labels residing in the aqueous phase or in the lipid bilayers by examining the EPR signal intensity as a function of microwave power. The power at which the measured signal amplitude is half-saturated, $P_{1/2}$, is proportional to the longitudinal relaxation rate of the spin-label. EPR power saturation data were collected on residues 46, 47, 48, 49, 50, 54, 55, 57, 59, 60, 61, 62, 64, 65, 66, 68, 69, 70, and 71 of the transmembrane domain, residues 5, 12, 15, 28, 29, 32, 34, 35, and 37 of the N-terminal domain, and residues 72, 76, 79, 81, 84, 89, 97, 102, 106, 107, 109, 117, and 129 of the C-terminal domain of KCNE1. Figure 6 shows an example of the power saturation data for spin-labeled V50C and E72C KCNE1. Inspection of the power saturation profile in Figure 6 indicates that the addition of NiEDDA to E72C KCNE1 has a dramatic effect on the power saturation curve, indicating that E72C is water accessible. Conversely, the power saturation profile of V50C indicates that the addition of O_2 (air) alters the relaxation profile much more than N_2 and NiEDDA, indicating that V50C is buried inside the hydrophobic phospholipid bilayer. The N_2 control experiments showed similar saturation results for the mutants. Table 1 shows the corresponding membrane depth parameters (φ) calculated according to eq 3 for all spin-labeled mutants. An increase in φ value indicates that the residue is buried more deeply in the membrane while negative φ values indicate the residue is accessible to the solvent. Spin-labeled mutants Y46C, V47C, L48C, M49C, V50C, F54C, G55C, F57C, L59C, G60C, I61C, M62C, S64C, Y65C, I66C, S68C, K69C, and K70C follow a trend as the depth parameter (φ) increases from 0.0 to 1.9 and then decreases again to −0.2 indicating that the predicted TMD is spanning the width of the lipid bilayers. The φ values for the C-terminus end vary between 0.0 to −1.5 and those for the N-terminus vary between 0.0 to −1.1, indicating that N-terminus is closer to the membrane surface when compared to the C-terminus. Residues K15C, S34C, and S84C have φ values ~0 in the N- and C-termini indicates that these residue are closer to or weakly interact with the membrane surface (Figure 7C). All of the remaining mutants in the N- and C-termini studied (Table 1 and Figure 7C) show that these residues are solvent accessible. From Table 1 and Figure 7C, it is clear that the KCNE1 TMD interacts strongly with the hydrophobic acyl chain of lipid bilayers and fully spans the width of the bilayer membrane. The membrane depth parameter and membrane depth in Table 1 and Figure 7C reveal that positions 46 and 70 are close to the surface of the lipid bilayer, while 59 is close to the center of lipid bilayers. The location of the TMD residues of KCNE1 (Table 1 and Figure 7C) is consistent with the length of the TMD from the published solution NMR structure and our recent EPR DEER study.[2,7,13] The φ values and overall membrane thickness obtained in this study are similar to those previously observed in the literature for transmembrane proteins.[44,45] The power saturation data shown in Table 1 are consistent with the CW-EPR line shape data (Figure 2) and side-chain mobility and motional parameters shown in Figures 3 and 4.

DISCUSSION

We previously demonstrated functional reconstitution of KCNE1 into POPC/POPG lipid bilayers and compared the conformations of KCNE1 in micelles and lipid bilayers.[12] Here we present a detailed study on the dynamics and topology of spin-labeled KCNE1 mutants using CW-EPR line shape analysis and CW-EPR power saturation experiments with respect to the membrane. Quantitative information about the structural dynamics and topology of KCNE1 in lipid bilayers is very important for understanding its function while interacting with KCNQ1 during K^+ channel gating. The data reported in this study provide a better understanding of side-chain motions and the locations of different segments of KCNE1 in lipid bilayers.

The prominent appearance of two motional components in the C-terminus of the KCNE1 sequence (Figure 2C) suggests that this segment of the protein may undergo multiple conformational states when interacting with the surface of the lipid bilayers as indicated by the effect of the addition of 30% sucrose on the EPR line shape (Figure 5). The comparison of single component EPR spectra observed in KCNE1 micelles samples (Figure S2) to the two major components observed in the spectra of KCNE1 in lipid bilayers also suggest that the protein may undergo two conformational states when interacting with the membrane. We speculate that POPC/POPG (3:1) lipid bilayers with anionic characteristics have a higher affinity to attract the positively charged KCNE1 segment (92–106) that may favor the stabilization of two protein conformations. Further studies with different lipid combinations may be needed to justify if these two conformations are an intrinsic property of KCNE1 or based on the choice of lipid. However, the second choice is less likely because most native membrane systems contain a mixture of PC and PG lipids.[12,15,16,29]

This motional behavior of the C-terminus is consistent with the solution NMR structure indicating disorder at the end of the C-terminus.[2] The inverse central line width has been proven to be a powerful, semi empirical parameter for the estimation of relative rotational mobility.[30,46,47] The empirical motional parameter (τ_0) is also known as the rotational correlation time (τ_c) in the case of intermediate-to-fast motional regime of EPR, where three distinct first-derivative lines are observed (Figure 4).[20] The rotational correlation time, τ_c, is the time necessary for the spin-label to rotate through an angle of 1 rad, so that shorter times (smaller values of τ_c) indicate faster motion. The higher mobility and lower motional parameter pattern of the C-terminus also suggests that this region is comparatively dynamic active.[2,48] The theoretically simulated rotational correlation times for both components (rigid and mobile) of EPR spectra (Figure S1 and Table S1) having higher values for the mutants (V50C and I66C) along the transmembrane domain and lower values for the mutants (F12C, D76C) along the extracellular region of KCNE1 are consistent with the empirical motional parameter of KCNE1 (Figure 4).

CW-EPR power saturation data presented in this study clearly indicate that the NMR-inferred KCNE1 TMD does indeed span the width of the lipid bilayer. The extracellular region of KCNE1 is solvent-exposed with some of the portions interacting with the membrane surface (Figure 7C). The power saturation data are consistent with the side-chain mobility and motional parameter pattern suggesting the C-terminus is more mobile and

flexible than the N-terminus. Previous studies indicated that the C-terminal domain of KCNE1 prevents channel inactivation and contributes to the modulation of KCNQ1, whereas the N-terminus of KCNE1 alters pH sensitivity and the pharmacological profile of the channel.[14,49–51] The variable motional and membrane interaction behavior of the KCNE1 sequence may favor the variable functional behavior of KCNE1. A recent rigid body docking study of the NMR-determined LMPG structure model of KCNE1 indicated that the extracellular helices (regions 12–23 and 92–106, see Figure 6A,B) are situated on or near the micelle surface.[2] The EPR power saturation data and the corresponding membrane depth parameters reported in this study have values close to zero (corresponding to sites 12, 15, 97, 106, 107) and are consistent with the rigid body docking model. These regions include an amphipathic helix spanning residues 12–23 and a net positively charged helix spanning residues 92–106 with an affinity for the negatively charged surface provided by the POPG lipids present in the membrane vesicles.[2] The observed depth parameter values of near zero corresponding to sites 34 and 84 suggest that these regions may be near the membrane surface. The flexible linkage of extracellular helices may allow structural adaptation to the local environment of KCNE1 under physiological conditions.[2] POPC/POPG lipids were used for this study since they are typically found in mammalian membranes.[12,15,16,29]

The KCNE1 segments with two different motional conformations in liposomes may have a higher functional relevance and favor the interaction of KCNE1 with KCNQ1 stabilizing the KCNE1/KCNQ1 complex.[2,7,52] The structural topology and dynamics model reported in this study are consistent with the POPC/POPG lipid bilayer width and their membrane surface properties.[12,13] However, the depth parameter values and dynamic flexibility may vary depending upon the length and choice of phospholipids used for the measurements.[53] Since the extracellular domain of KCNE1 undergoes two major conformations (as evidenced by two major CW-EPR spectral components, Figure 2), the EPR power saturation depth parameters corresponding to the sites in this domain might reflect the average saturation behavior of the multiple components.[54] Therefore, the topological information obtained corresponding to the sites in the extracellular domain may be more qualitative.

CONCLUSION

The side-chain motion and structural topology of the membrane-bound KCNE1 protein in POPC/POPG lipid bilayered vesicles was investigated using CW-EPR spectroscopy. Spectral line shape data analysis indicates that the TMD of KCNE1 is less mobile when compared to the C- and N-terminal domains. Also, the C-terminus is more mobile, when compared to the N-terminus. The CW-EPR power saturation data indicate that residues 45–71 of the transmembrane domain of KCNE1 are located inside the membrane, and L59 is buried the deepest. The results of this work also indicate that the N-terminus domain interacts more closely with the membrane surface than the C-terminus. Since the C-terminus is more mobile, this KCNE1 region may interact more favorably with the KCNQ1 channel.

Supplementary Material

Refer to Web version on PubMed Central for supplementary material.

Acknowledgments

Funding

This work was supported by National Institutes of Health Grants R01 GM108026 (to GAL), and R01 DC007416 (to CRS). Funding was also provided by National Science Foundation (NSF) Grant CHE-1305664 (to GAL).

ABBREVIATIONS

LQTS	long QT syndrome
TMD	transmembrane domain
NMR	nuclear magnetic resonance
SDSL	site-directed spin labeling
CW-EPR	continuous wave electron paramagnetic resonance
DEER	double electron-electron resonance
IMD	imidazole
IPTG	isopropyl-1-thio-D-galactopyranoside
SDS-PAGE	sodium dodecyl sulfatepolyacrylamide gelelectrophoresis
LMPG	1-myristoyl-2-hydroxy-*sn*-glycero-3-phospho-(1′-*rac*-glycerol) (sodium salt)
MTSL	1-oxyl-2,2,5,5-tetramethyl-pyrroline-3-methylmethanethiosulfonate spin label
POPC	1-palmitoyl-2-oleoyl-*sn*-glycero-3-phosphocholine
POPG	1-pal-mitoyl-2-oleoyl-*sn*-glycero-3-phospho-(1′-*rac*-glycerol) (sodium salt)
LMPG	1-myristoyl-2-hydroxy-*sn*-glycero-3-phospho-(1′-*rac*-glycerol) (sodium salt)
CD	circular dichroism

References

1. Koichi N, Yoshihiro K. KCNE1 and KCNE3 Stabilize and/or Slow Voltage Sensing S4 Segment of KCNQ1 Channel. J Gen Physiol. 2007; 130:269–281. [PubMed: 17698596]
2. Kang C, Tian C, Sonnichsen FD, Smith JA, Meiler J, George AL Jr, Vanoye CG, Kim HJ, Sanders CR. Structure of KCNE1 and implications for how it modulates the KCNQ1 potassium channel. Biochemistry. 2008; 47:7999–8006. [PubMed: 18611041]
3. Tai KK, Goldstein SAN. The conduction pore of a cardiac potassium channel. Nature. 1998; 391:605–608. [PubMed: 9468141]
4. Uysal S, Vasquez V, Tereshko V, Esaki K, Fellouse FA, Sidhu SS, Koide S, Perozo E, Kossiakoff A. Crystal structure of full-length KcsA in its closed conformation. Proc Natl Acad Sci U S A. 2009; 106:6644–6649. [PubMed: 19346472]
5. Ketchum KA, Joiner WJ, Sellers AJ, Kaczmarek LK, Goldstein SAN. A New Family of Outwardly Rectifying Potassium Channel Proteins with 2 Pore Domains in Tandem. Nature. 1995; 376:690–695. [PubMed: 7651518]

6. Herlyn H, Zechner U, Oswald F, Pfeufer A, Zischler H, Haaf T. Positive selection at codon 38 of the human *KCNE1* (minK) gene and sporadic absence of 38Ser-coding mRNAs in Gly38Ser heterozygotes. BMC Evol Biol. 2009; 9:188. [PubMed: 19660109]
7. Tian C, Vanoye CG, Kang C, Welch RC, Kim HJ, George AL, Sanders CR. Preparation, Functional Characterization, and NMR Studies of Human KCNE1, a Voltage-Gated Potassium Channel Accessory Subunit Associated with Deafness and Long QT Syndrome. Biochemistry. 2007; 46:11459–11472. [PubMed: 17892302]
8. Wang Z, Fermini B, Nattel S. Rapid and slow components of delayed rectifi er current in human atrial myocytes. Cardiovasc Res. 1994; 28:1540–1546. [PubMed: 8001043]
9. Harmer SC, Tinker A. The role of abnormal trafficking of KCNE1 in long QT syndrome 5. Biochem Soc Trans. 2007; 35:1074–1076. [PubMed: 17956282]
10. Zhou HX, Cross TA. Influences of Membrane Mimetic Environments on Membrane Protein Structures. Annu Rev Biophys. 2013; 42:361–392. [PubMed: 23451886]
11. Jao CC, Hegde BG, Chen J, Haworth IS, Langen R. Structure of membrane-bound alpha-synuclein from site-directed spin labeling and computational refinement. Proc Natl Acad Sci U S A. 2008; 105:19666–19671. [PubMed: 19066219]
12. Coey AT, Sahu ID, Gunasekera TS, Troxel KR, Hawn JM, Swartz MS, Wickenheiser MR, Reid RJ, Welch RC, Vanoye CG, Kang CB, Sanders CR, Lorigan GA. Reconstitution of KCNE1 into Lipid Bilayers: Comparing the Structural, Dynamic, and Activity Differences in Micelle and Vesicle Environments. Biochemistry. 2011; 50:10851–10859. [PubMed: 22085289]
13. Sahu ID, Kroncke BM, Zhang R, Dunagan MM, Smith HJ, Craig A, McCarrick RM, Sanders CR, Lorigan GA. Structural Investigation of the Transmembrane Domain of KCNE1 in Proteoliposomes. Biochemistry. 2014; 53:6392–6401. [PubMed: 25234231]
14. Tapper AR, George AL. MinK subdomains that mediate modulation of and association with KvLQT1. J Gen Physiol. 2000; 116:379–390. [PubMed: 10962015]
15. Barrett PJ, Song Y, Van Horn WD, Hustedt EJ, Schafer JM, Hadziselimovic A, Beel AJ, Sanders CR. The Amyloid Precursor Protein Has a Flexible Transmembrane Domain and Binds Cholesterol. Science. 2012; 336:1168–1171. [PubMed: 22654059]
16. Sahu ID, McCarrick RM, Troxel KR, Zhang R, Smith JH, Dunagan MM, Swartz MS, Rajan PV, Kroncke BM, Sanders CR, Lorigan GA. DEER EPR measurement for Membrane Protein Structures via Bifunctional Spin Labels and Lipodisq Nanoparticles. Biochemistry. 2013; 52:6627–6632. [PubMed: 23984855]
17. Bates IR, Boggs JM, Feix JB, Harauz G. Membrane-anchoring and charge effects in the interaction of myelin basic protein with lipid bilayers studied by site-directed spin labeling. J Biol Chem. 2003; 278:29041–29047. [PubMed: 12748174]
18. Boggs JM, Moscarello MA. Effect of Basic-Protein from Human Central Nervous-System Myelin on Lipid Bilayer Structure. J Membr Biol. 1978; 39:75–96. [PubMed: 204786]
19. Eletr S, Keith AD. Spin-Label Studies of Dynamics of Lipid Alkyl Chains in Biological-Membranes – Role of Unsaturated Sites. Proc Natl Acad Sci U S A. 1972; 69:1353–1357. [PubMed: 4338592]
20. Klug CS, Feix JB. Methods and Applications of Site-Directed Spin Labeling EPR Spectroscopy. Methods Cell Biol. 2008; 84:617–658. [PubMed: 17964945]
21. Toledo Warshaviak DT, Khramtsov VV, Cascio D, Altenbach C, Hubbell WL. Structure and dynamics of an imidazoline nitroxide side chain with strongly hindered internal motion in proteins. J Magn Reson. 2013; 232:53–61. [PubMed: 23694751]
22. Schneider, DJ.; Freed, JH. Calculating slow motional magnetic resonance spectra: a user's guide. In: Berlinger, LJ., editor. Biol Magn Reson. Plenum Publishing; New York: 1989.
23. Budil DE, Lee S, Saxena S, Freed JH. Nonlinear-Least-Squares Analysis of Slow-Motion EPR Spectra in One and Two Dimensions Using a Modified Levenberg-Marquardt Algorithm. J Magn Reson Ser A. 1996; 120:155–189.
24. Averill DF, Smith DL, Legg JI. 5-Coordinate, Square-Pyramidal Chelate Complexes of a Novel Tetradentate Amino-Acid Like Ligand. Inorg Chem. 1972; 11:2344–2349.

25. Rauch ME, Ferguson CG, Prestwich GD, Cafiso DS. Myristoylated alanine-rich C kinase substrate (MARCKS) sequesters spin-labeled phosphatidylinositol 4,5-bisphosphate in lipid bilayers. J Biol Chem. 2002; 277:14068–14076. [PubMed: 11825894]
26. Altenbach C, Greenhalgh DA, Khorana HG, Hubbell WL. A collision gradient method to determine the immersion depth of nitroxides in lipid bilayers: application to spin-labeled mutants of bacteriorhodopsin. Proc Natl Acad Sci U S A. 1994; 91:1667–1671. [PubMed: 8127863]
27. Frazier AA, Wisner MA, Malmberg NJ, Victor KG, Fanucci GE, Nalefski EA, Falke JJ, Cafiso DS. Membrane orientation and position of the C2 domain from cPLA2 by site-directed spin labeling. Biochemistry. 2002; 41:6282–6292. [PubMed: 12009889]
28. Kohout SC, Corbalan-Garcia S, Gomez-Fernandez JC, Falke JJ. C2 domain of protein kinase C alpha: elucidation of the membrane docking surface by site-directed fluorescence and spin labeling. Biochemistry. 2003; 42:1254–1265. [PubMed: 12564928]
29. Song Y, Hustedt EJ, Brandon S, Sanders CR. Competition Between Homodimerization and Cholesterol Binding to the C99 Domain of the Amyloid Precursor Protein. Biochemistry. 2013; 52:5051–5064. [PubMed: 23865807]
30. Hubbell WL, McHaourab HS, Altenbach C, Lietzow MA. Watching proteins move using site-directed spin labeling. Structure. 1996; 4:779–783. [PubMed: 8805569]
31. Sahu ID, McCarrick RM, Lorigan GA. Use of Electron Paramagnetic Resonance to Solve Biochemical Problems. Biochemistry. 2013; 52:5967–5984. [PubMed: 23961941]
32. Jeschke G, Bender A, Schweikardt T, Panek G, Decker H, Paulsen H. Localization of the N-terminal domain in light-harvesting chlorophyll a/b protein by EPR measurements. J Biol Chem. 2005; 280:18623–18630. [PubMed: 15755729]
33. Mchaourab, HS.; Perozo, E. Determination of Protein Folds and Conformational Dynamics Using Spin-Labeling EPR Spectroscopy. In: Berliner, L.; Eaton, G.; Eaton, S., editors. Biol Magn Reson. Springer; New York: 2002. p. 185-247.
34. Perozo E, Cortes DM, Cuello LG. Three-dimensional architecture and gating mechanism of a K+ channel studied by EPR spectroscopy. Nat Struct Biol. 1998; 5:459–469. [PubMed: 9628484]
35. Vasquez V, Sotomayor M, Marien Cortes D, Roux B, Schulten K, Perozo E. Three-dimensional architecture of membrane-embedded MscS in the closed conformation. J Mol Biol. 2008; 378:55–70. [PubMed: 18343404]
36. Altenbach C, Flitsch SL, Khorana HG, Hubbell WL. Structural studies on transmembrane proteins. 2. Spin labeling of bacteriorhodopsin mutants at unique cysteines. Biochemistry. 1989; 28:7806–7812. [PubMed: 2558712]
37. Kusnetzow AK, Altenbach C, Hubbell WL. Conformational states and dynamics of rhodopsin in micelles and bilayers. Biochemistry. 2006; 45:5538–5550. [PubMed: 16634635]
38. Oh KJ, Singh P, Lee K, Foss K, Lee S, Park M, Lee S, Aluvila S, Park M, Singh P, Kim RS, Symersky J, Walters DE. Conformational Changes in BAK, a Pore-forming Proapoptotic Bcl-2 Family Member, upon Membrane Insertion and Direct Evidence for the Existence of BH3-BH3 Contact Interface in BAK Homo-oligomers. J Biol Chem. 2010; 285:28924–28937. [PubMed: 20605789]
39. Nguyen PA, Soto CS, Polishchuk A, Caputo GA, Tatko CD, Ma C, Ohigashi Y, Pinto LH, DeGrado WF, Howard KP. pH-induced conformational change of the influenza M2 protein C-terminal domain. Biochemistry. 2008; 47:9934–9936. [PubMed: 18754675]
40. Xu Q, Kim M, Ho KWD, Lachowicz P, Fanucci GE, Cafiso DS. Membrane hydrocarbon thickness modulates the dynamics of a membrane transport protein. Biophys J. 2008; 95:2849–2858. [PubMed: 18586842]
41. Yu L, Wang W, Ling S, Liu S, Xiao L, Xin Y, Lai C, Xiong Y, Zhang L, Tian C. CW-EPR studies revealed different motional properties and oligomeric states of the integrin beta(1a) transmembrane domain in detergent micelles or liposomes. Sci Rep. 2015; 5:7848. [PubMed: 25597475]
42. Li Q, Wanderling S, Sompornpisut P, Perozo E. Structural basis of lipid-driven conformational transitions in the KvAP voltage-sensing domain. Nat Struct Mol Biol. 2014; 21:160–166. [PubMed: 24413055]

43. Lopez CJ, Fleissner MR, Guo Z, Kusnetzow AK, Hubbell WL. Osmolyte perturbation reveals conformational equilibria in spin-labeled proteins. Protein Sci. 2009; 18:1637–1652. [PubMed: 19585559]
44. Klug CS, Su WY, Feix JB. Mapping of the residues involved in a proposed beta-strand located in the ferric enterobactin receptor FepA using site-directed spin-labeling. Biochemistry. 1997; 36:13027–13033. [PubMed: 9335564]
45. Fanucci GE, Cadieux N, Piedmont CA, Kadner RJ, Cafiso DS. Structure and dynamics of the beta-barrel of the membrane transporter BtuB by site-directed spin labeling. Biochemistry. 2002; 41:11543–11551. [PubMed: 12269798]
46. Hubbell WL, Cafiso DS, Altenbach C. Identifying conformational changes with site-directed spin labeling. Nat Struct Biol. 2000; 7:735–739. [PubMed: 10966640]
47. Hubbell WL, Gross A, Langen R, Lietzow MA. Recent advances in site-directed spin labeling of proteins. Curr Opin Struct Biol. 1998; 8:649–656. [PubMed: 9818271]
48. Dyson HJ, Wright PE. Intrinsically unstructured proteins and their functions. Nat Rev Mol Cell Biol. 2005; 6:197–208. [PubMed: 15738986]
49. Splawski I, TristaniFirouzi M, Lehmann MH, Sanguinetti MC, Keating MT. Mutations in the hminK gene cause long QT syndrome and suppress I-Ks function. Nat Genet. 1997; 17:338–340. [PubMed: 9354802]
50. Heitzmann D, Koren V, Wagner M, Sterner C, Reichold M, Tegtmeier I, Volk T, Warth R. KCNE beta subunits determine pH sensitivity of KCNQ1 potassium channels. Cell Physiol Biochem. 2007; 19:21–32. [PubMed: 17310097]
51. Peretz A, Schottelndreier H, Aharon-Shamgar LB, Attali B. Modulation of homomeric and heteromeric KCNQ1 channels by external acidification. J Physiol. 2002; 545:751–766. [PubMed: 12482884]
52. Xu Y, Wang Y, Meng XY, Zhang M, Jiang M, Cui M, Tseng GN. Building KCNQ1/KCNE1 Channel Models and Probing their Interactions by Molecular-Dynamics Simulations. Biophys J. 2013; 105:2461–2473. [PubMed: 24314077]
53. Kandasamy SK, Larson RG. Molecular dynamics simulations of model trans-membrane peptides in lipid bilayers: A systematic investigation of hydrophobic mismatch. Biophys J. 2006; 90:2326–2343. [PubMed: 16428278]
54. Oh KJ, Altenbach C, Collier RJ, Hubbell WL. Site-directed spin labeling of proteins. Applications to diphtheria toxin. Methods in molecular biology (Clifton, NJ). 2000; 145:147–169.

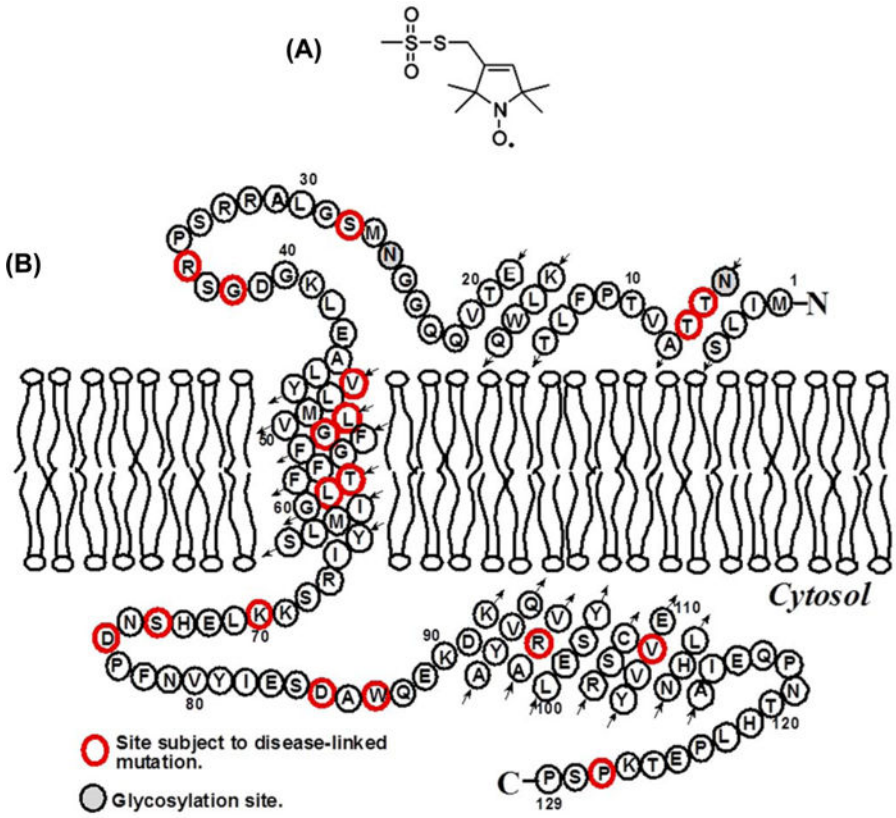

Figure 1.

Schematic representation of MTSL (A), the proposed topology of the KCNE1 sequence in lipid bilayers (B), amino acid sequence of wild-type KCNE1 (C). The red-colored sites were replaced with MTSL spin-labels.

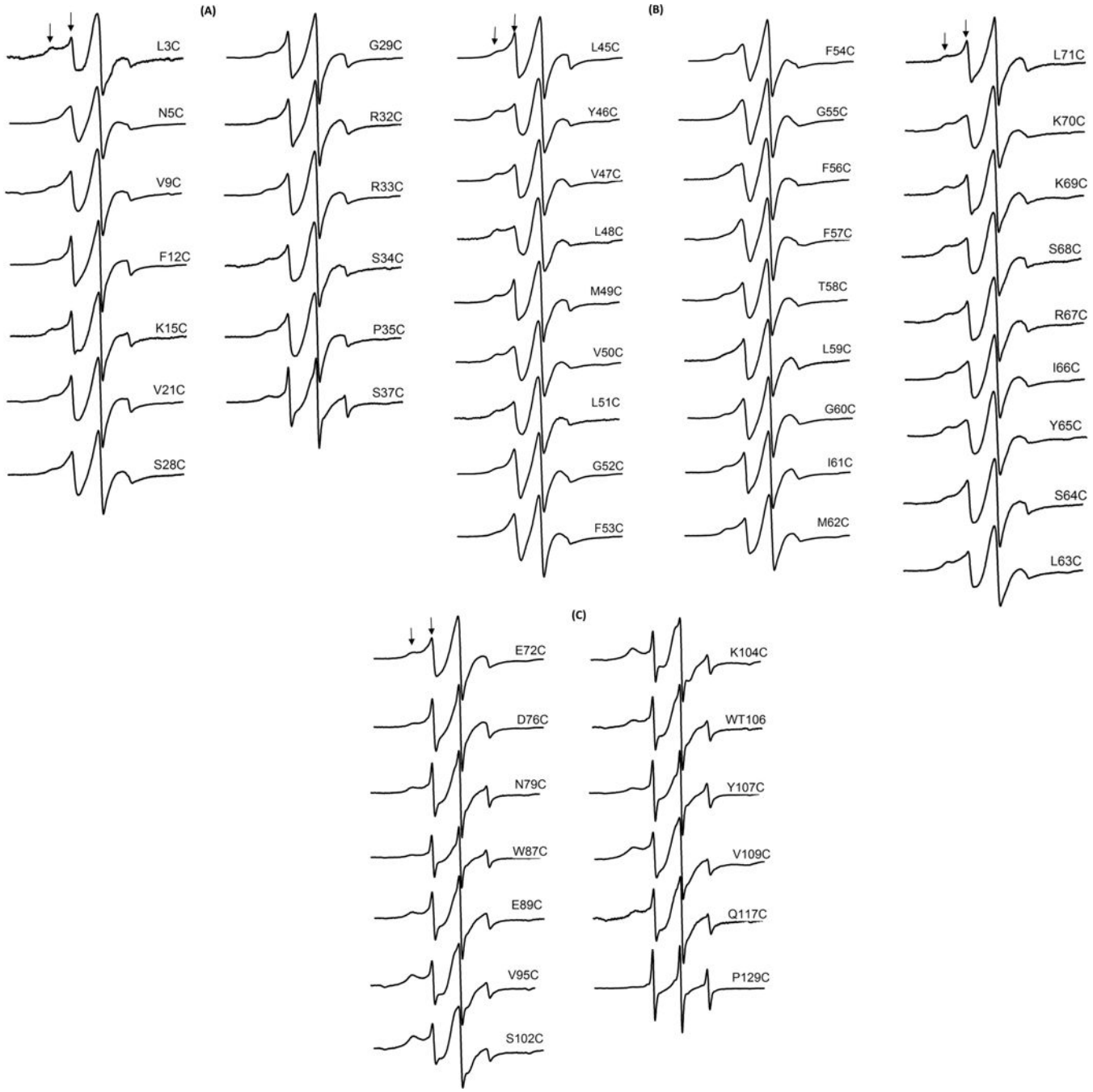

Figure 2.

CW-EPR spectra on KCNE1 mutants in POPC/POPG bilayered vesicles at pH 6.5: (A) The N-terminus, (B) The transmembrane domain, and (C) The C-terminus. Spectra were normalized to the highest spectral intensity.

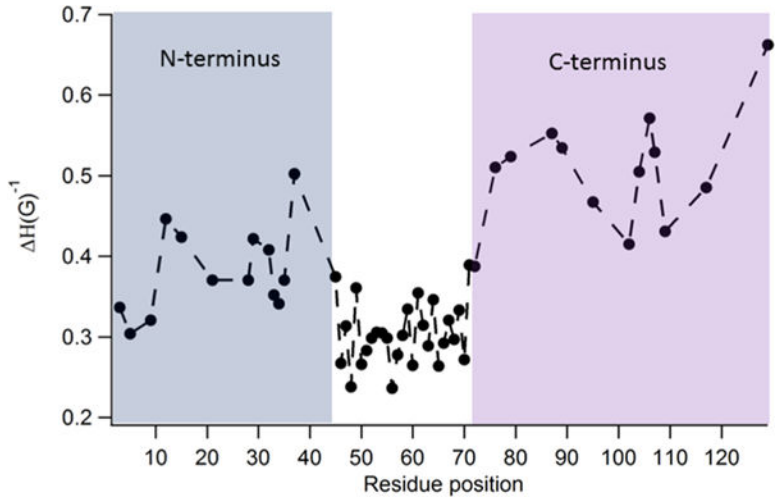

Figure 3.

Plot of inverse central EPR resonance line width ($m_I = 0$) as a function of residue position, as calculated from the CW-EPR spectra of KCNE1 mutants shown in Figure 2.

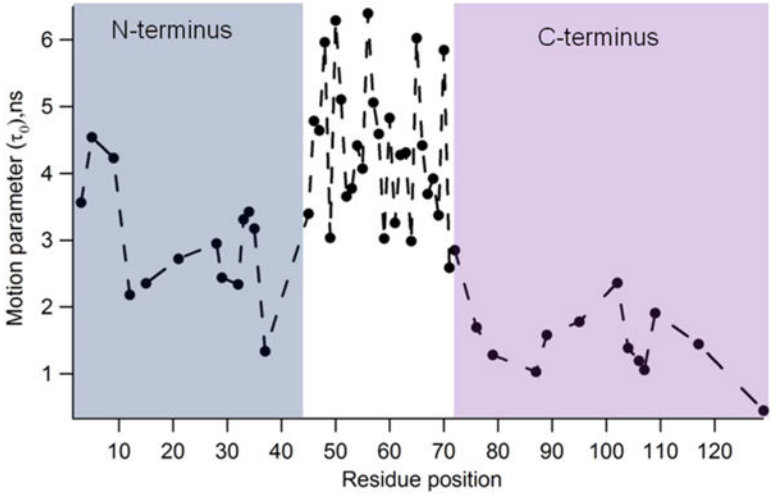

Figure 4.

Plot of the motional parameter (τ_0) as a function of residue position calculated from the CW-EPR spectra of KCNE1 mutants shown in Figure 2.

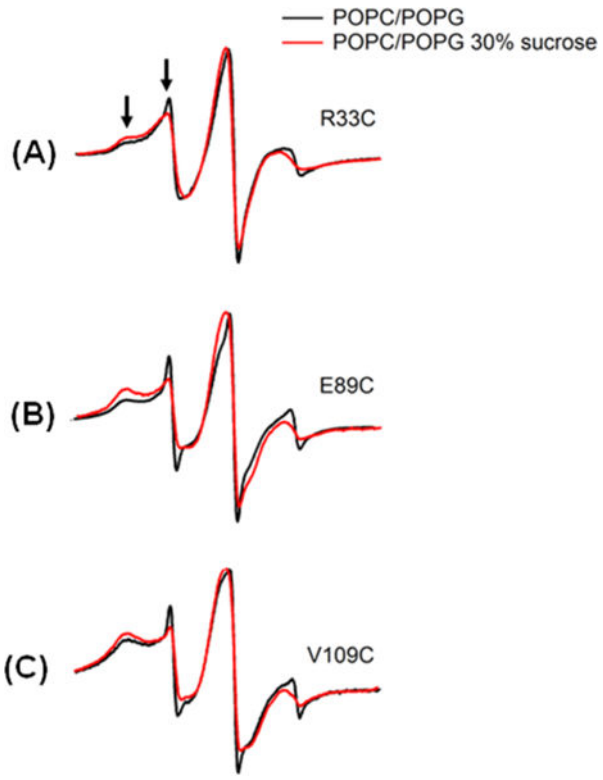

Figure 5.

Effect of osmolyte perturbation on the motion of spin-label KCNE1 mutants: (A) R33C (N-terminus), (B) E89C (C-terminus), and (C) V109C (C-terminus). 30% sucrose was used as osmolytes. Spectra were normalized to the highest spectral intensity. The left arrows reflect rigid/slower components, while the right arrows shows higher/faster motional components.

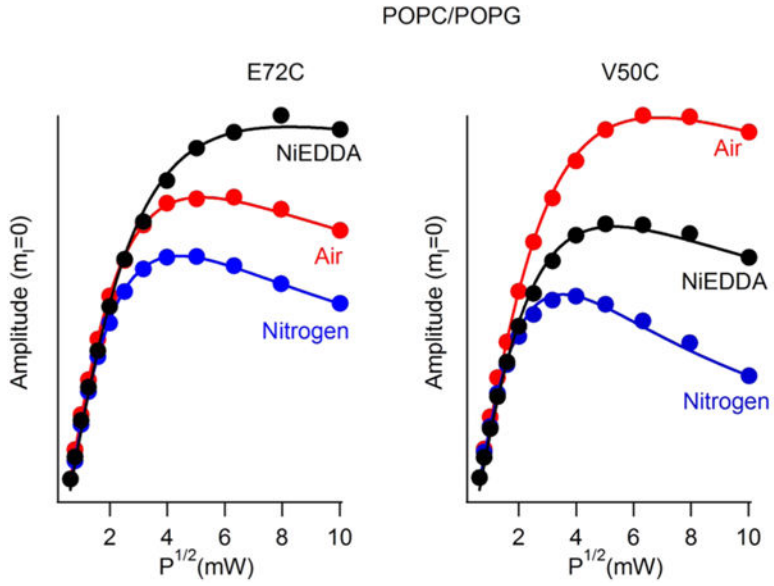

Figure 6.

Examples of EPR power saturation curves from KCNE1 in POPC/POPG lipid bilayered vesicles at 295 K. Mutation E72C is at a site outside the lipid bilayer, while the V50C site is part of the transmembrane domain. The low power amplitude for each of the conditions was rescaled to a common value.

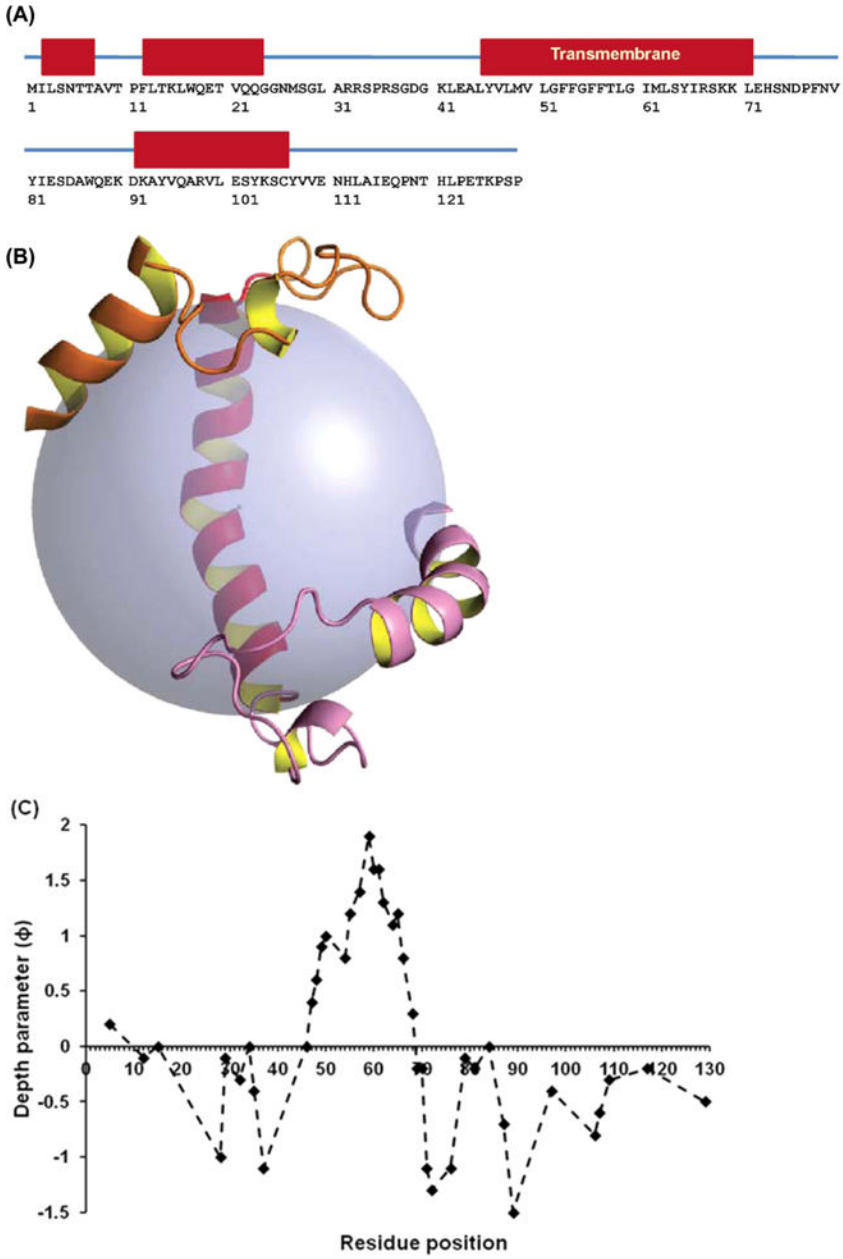

Figure 7.

(A) Location of α-helices in the three-dimensional NMR structure of KCNE1 represented by red boxes,[2] (B) rigid body docking model of NMR-determined LMPG micelle structure with helical regions interacting with micelle surface,[2] (C) membrane depth parameter (φ) as a function of KCNE1 residue position in POPC/POPG lipid bilayered vesicles at 295 K. The uncertainty in φ value is ±0.2–0.4, arising from the error present in $P_{1/2}$ value measurements caused by multiple conformations of MTSL spin label rotamers and multiple conformational states of the protein while interacting with the membrane.

Table 1

Depth Parameter (φ) and Membrane Depth for Different Spin-Labeled KCNE1 Residues in POPC/POPG Bilayered Vesicles[a]

label position	depth parameter (φ)	membrane depth (Å)
N5C	0.2	
F12C	−0.1	
K15C	0.0	
S28C	−1.0	
G29C	−0.1	
R32C	−0.3	
S34C	0.0	
P35C	−0.4	
S37C	−1.1	
Y46C	0.0	2.1
V47C	0.4	4.4
L48C	0.6	5.3
M49C	0.9	7.3
V50C	1.0	7.8
F54C	0.8	6.7
G55C	1.2	9.1
F57C	1.4	10.2
L59C	1.9	12.9
G60C	1.6	11.2
I61C	1.6	11.2
M62C	1.3	9.2
S64C	1.1	8.4
Y65C	1.2	8.9
I66C	0.8	6.5
S68C	0.3	4.1
K69C	−0.2	1.2
K70C	−0.2	1.1
L71C	−1.1	
E72C	−1.3	
D76C	−1.1	
N79C	−0.1	
Y81C	−0.2	
S84C	0.0	
W87C	−0.7	
E89C	−1.5	
A97C	−0.4	
C106	−0.8	
Y107C	−0.6	

label position	depth parameter (φ)	membrane depth (Å)
V109C	−0.3	
Q117C	−0.2	
P129C	−0.5	

[a] The uncertainty in the membrane depth measurement is ±2–3 Å, arising from the error present in the measurement of φ values.